Experimental analysis of the scaled DTU10MW TLP floating wind turbine with different control strategies

F.J. Madsen [a], T.R.L. Nielsen [a], T. Kim [a, b, *], H. Bredmose [a], A. Pegalajar-Jurado [a], R.F. Mikkelsen [a], A.K. Lomholt [a], M. Borg [a, c], M. Mirzaei [a, d], P. Shin [e]

[a] DTU Wind Energy, Kgs. Lyngby, Denmark
[b] Centre for Renewable Energy Systems Technology (CREST), Wolfson School of Mechanical, Electrical and Manufacturing Engineering, Loughborough University, Loughborough, LE11 3TU, UK
[c] Borg R&D, Malta
[d] Vestas Wind System, Aarhus, Denmark
[e] Wind Energy Laboratory, Jeju Global Research Center, Korea Institute of Energy Research (KIER), Jeju, Republic of Korea

ARTICLE INFO

ABSTRACT

The experimental testing of a Tension Leg Platform (TLP) floating wind turbine at 1:60 scale in wind and waves with a pitch-regulated 10 MW wind turbine is presented. The floating wind turbine was tested with three different control configurations: two closed-loop controllers and one open-loop controller. The experimental setup and program is described in this paper, and system identification and the responses of the floater to hydrodynamic loading are analysed and compared for the different control strategies. It was observed that negative aerodynamic damping for the onshore controller resulted in high oscillations in blade pitch, yielding an increased response in surge for all wave types. It was also observed that the surge motion governed the mooring line tensions, thus the onshore controller yielded the highest tensions in the front mooring line. Further the shutdown cases of the offshore controller led to larger surge displacement when the shutdown was initialized right before the wave impact.

© 2020 Elsevier Ltd. All rights reserved.

1. Introduction

European Union (EU) made a plan to meet 20% energy consumption from renewable energy source by 2020 in 2006 [1]. A new target of at least 27% of EU's energy consumption from renewable energy by 2030 has been agreed in 2014. In order to meet the target the share of renewable energy in the electricity would increase from 21 percent to 45 percent by 2030 [2]. The considered renewable sources are wind, solar, wave, tidal, hydro, geothermal, biomass, etc. Among them wind energy has become the most promising renewable energy source. The global wind energy installed capacity reached 591 GW in 2018 and in total 51.3 GW of new wind farm capacity was installed in 2018, where 4.49 GW, which is approximately 20% of growth rate, was covered by offshore wind energy. Especially in Europe in total 409 new offshore wind turbines were connected to the grid in 2018 and has approximately 18.5 GW installed capacity in the offshore sector [3].

The next step of offshore wind energy will be DEEP WATER, i.e. water depths greater than 50 m, meaning that floating wind turbine concepts must be developed. In response to this challenge the first commercial floating wind farm, Hywind Scotland Pilot Park, has been successfully installed and operated since 2017. Here the Hywind type spar buoy floater is applied with a 6 MW SWT-6.0-154 wind turbine. However, the technology is still at early stage to achieve commercial and large-scale deployment. It requires the technological breakthroughs from wind turbines, control system, foundations, mooring and anchors, electrical infrastructures, installations, O&M, design standard, design tools, etc. [4,5].

There are large efforts to reduce risks of technology challenges and to identify innovations through the Floating Wind Joint Industry Project which is a collaborative R&D project. From this project, the knowledge of the key technology challenges and innovation needs for electrical systems, mooring systems, infrastructure and logistics are investigated [6]. Additionally, the second phase of the project, which aims to build knowledge on wind turbine requirements, foundation scaling, installation and maintenance, monitoring and inspection, is on-going. Furthermore,

research on developing floating wind turbine system design tools has been conducted and the developed numerical design tools are verified against other numerical results [7,8]. Since floating wind turbine concepts are in the prototype stage there are not enough experimental data to use for code validations. Recently, few experimental studies with small scale floating wind turbine concepts have been performed [9–11]. Only few experimental tests considered matching the aerodynamic thrust and controlling blade pitch on the rotor. From Ref. [9,11] it is clearly seen how different controller settings affect the floating wind turbine responses. DTU also demonstrated small scaled floating wind turbine basin tests with different types of floater designs and blade pitch control [12–15].

This paper extended the one of previous DTU experimental test performed by Hansen and Laugesen [16] by including a newly designed TLP floater and active blade pitch control. The small scale experimental tests are challenging, because of contrasting physical scaling laws for aerodynamic and hydrodynamic loads. In addition, the reproduced environmental conditions will have an impact on the relevant dynamics and loading captured in the laboratory tests. In this paper a 1:60 scaled DTU10MW Reference Wind Turbine model, where the rotor was redesigned to deliver the right Froude scaled thrust at the low Reynolds number [17], is applied with the basic DTU Wind Energy controller [18]. The main purpose of this test campaign is to understand dynamic responses governed by wave, aerodynamics, and control system. Moreover, the test results are able to be used to validate numerical tools for a floating wind turbine system design. Therefore the tests are conducted to establish a data set in a number of wave climates such as regular, irregular, and focused wave groups, both with and without wind. Additionally, emergency shutdown events with extreme wave condition, focused wave, were tested to analyse large surge effects condition driven by controller.

In the following the experimental setup during the test campaign will be described followed by a section on how the DTU Wind Energy controller was implemented. Next a validation of wind and waves, together with test and corrections on the performance of rotor thrust and decay tests are presented. Selected results highlighting the difference in behaviour of the floating wind turbine is shown based on three controller versions. This will be treated in both regular, irregular and focused waves, where the latter includes shutdown cases of the turbine.

2. Model concept

The TLP concept, developed by Korea Institute of Energy Research (KIER), consists of a floater body with a slender transition piece connecting the tower base to the floater body. Three outgoing spokes are mounted on the floater body, where the taunt mooring lines are attached. The stability of the concept is achieved through the excess buoyancy of the platform, thus the tension in the mooring lines. Fig. 1 shows the model-scaled floating wind turbine.

2.1. The 1:60 scale physical model

A full scale TLP was designed by KIER based on the Ultimate Limit State (ULS) loads on the DTU 10 MW Reference Wind Turbine (RWT) at the tower base. A 1:60 scaled model of the TLP concept was then developed based on the full-scale design to support the scaled DTU 10 MW Reference Wind Turbine (RWT) [19] for the experimental campaign [20].

As in the previous test campaigns ([14,21]), the Froude scaling law, with a geometric scaling ratio of 1:60, was applied to create the physical scaled model, following the work of [10,22]. It is known that the surface waves are primarily governed by the Froude
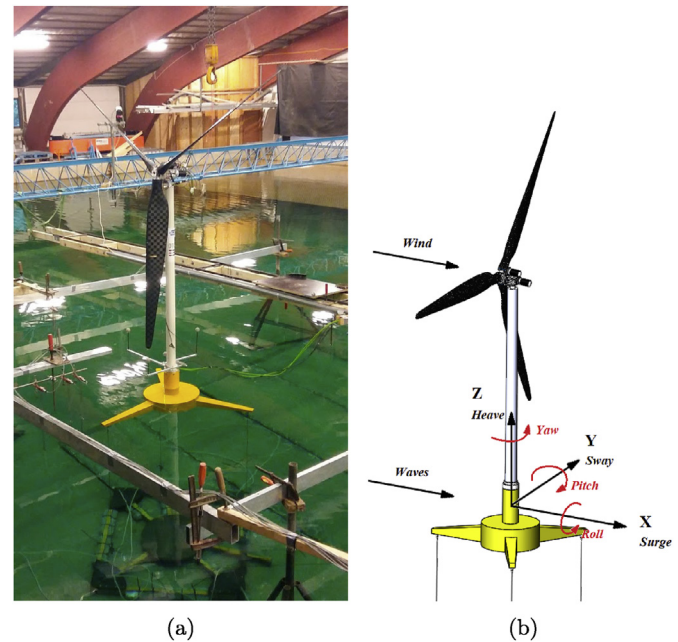

Fig. 1. The TLP floating wind turbine concept. (a): the full TLP floating wind turbine model. (b): the global coordinate system and degrees of freedom of the floating wind turbine.

number, *Fr*, and hence it is common practice to preserve this number in model tests of offshore structures and floating bodies.

The key parameters of the DTU 10 MW RWT, as described in Ref. [19], were Froude-scaled with the length scale ratio of $Sr = 60$. It introduces a significant issue that a geometrical scaling of the rotor will not give the correct aerodynamic performance of the blades due to the large dissimilitude in Reynolds number, *Re*, since the rotor aerodynamics are mainly governed by *Re*. This will lead to a reduction in the aerodynamic thrust and mechanical power, where especially the first is of great importance for the overall dynamics of the floating wind turbine. Hence, the rotor was redesigned in model scale using a steady thrust-matched rotor design, in order to deliver the right thrust at the low *Re*. Moreover effort was put into matching the tip speed ratio correctly and scaling the mass of the blades. The work of designing the thrust-matched blades is described in Ref. [17] and is characterized by an increase in chord length of 75% to achieve the needed lift at the low *Re*. This scaled rotor is identical to the one applied in previous campaigns ([14,21]) and the manufacturing process is described in Ref. [16].

The hub and nacelle of the scaled wind turbine model is much more simple in its composition compared to full scale, as the number of components is reduced significantly. The main functions of the hub and nacelle are to contain the motors, for control torque and blade pitch, whilst limiting the model weight, since the Froude scaling impose strong limitations on the allowable structural mass in model scale. Two JVL MAC050 servomotors were used, one for torque control and one for blade pitch control. More details about the nacelle and hub system are described in Ref. [14].

Tables 1 and 2 provide the main properties of the model scaled system. The corresponding full scale values of the model dimensions and masses can be obtained by multiplying the model scale values with the scaling factors $\frac{\rho_p}{\rho_m} Sr$ and $\frac{\rho_p}{\rho_m} Sr^3$ respectively, driven by the Froude scaling method, where ρ_p and ρ_m are the water densities in full and model scale respectively. The details on the scaling method are described in Refs. [22]. The mooring lines used in this study were Dyneema® fiber ropes with diameter of 2.2 mm

Table 1
The scaled TLP wind turbine masses.

| Element	Symbol	Model scale value
Nacelle + hub mass	$m_{nacelle} + m_{hub}$	2.896 kg
Blade mass	m_{blade}	0.200 kg
Tower mass	m_{tower}	2.250 kg
Transition piece mass	$m_{trans,dry}$	2.400 kg
Floater mass	m_{float}	9.900 kg
Spoke mass	m_{spoke}	1.400 kg
Total model mass	m_{tot}	22.246 kg

and breaking load of around 990 kg, due to the high tensile strength to weight ratio. The stiffness of the mooring lines was measured to be $EA_{moor} = 97.86 \cdot 10^3$ N.

3. Experimental setup

The experimental campaigns were carried out at DHI in a large 30 m × 20 m basin with a water depth of 3 m. Fig. 2 shows a top view of the basin, which also illustrates the experimental setup. For consistency the setup was chosen to follow the setup of previous test campaigns ([14,21]). The wave basin consists of 60 individual wave paddles, a, installed on the front side of the basin which enable creation of unidirectional waves, misaligned waves and directionally spread waves. In the opposite end of the wave paddles a passive parabolic wave absorber, c, is placed which minimizes the reflection of the waves. Furthermore a foam is placed along the sides of the basin, in order to reduce the transversal reflection of the waves. The floater, g, was installed 4 m from the wave paddles.

An open jet wind generator, b, with an outlet area of 4 m× 4 m was placed on the front side above the wave makers. It consists of six identical units with a fan in each that blows air laterally into a chamber, then guide vanes turns the flow 90° into the main wave direction. More details on the wind generator design can be found in Ref. [14,21].

Multiple sensors were installed on the wind turbine and all the signals were captured by a data acquisition device, d, which was situated on the control bridge, f, from where the experiments were
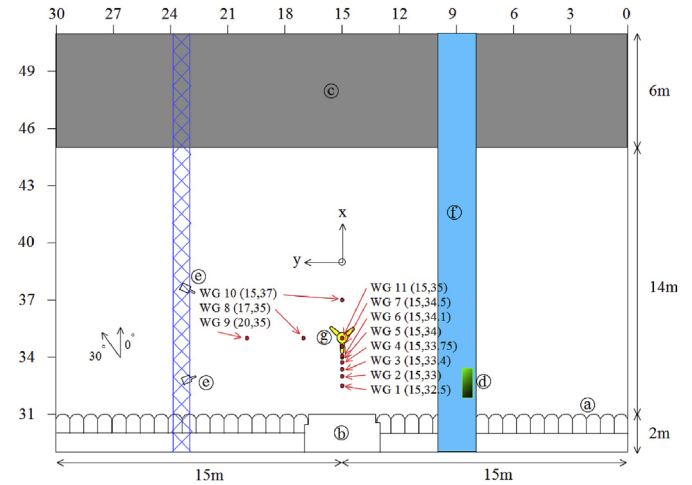
Fig. 2. Top view of the wave basin and the experimental setup.

controlled and monitored. Wave gauges (WG) were placed in the water to measure the wave elevation at eleven different locations in the basin, as shown in Fig. 2.

The six degrees of freedom floater motion was measured with a motion tracking system, Qualisys, which is a setup consisting of two cameras, e, and tracking markers rigidly mounted at the tower bottom point. The inline and lateral shear force were measured using a shear force gauge installed between the nacelle and the tower top. In addition the inline and transverse acceleration in the nacelle were logged with two one degree of freedom accelerometers. The torque of the shaft servo motor governing the rotational speed was logged, together with the rotational speed of the shaft and the collective blade pitch.

Lastly a foundation to anchor the mooring lines was fixed on the basin bottom by the use of concrete blocks and lead bars which do not affect the wave motions during the experiments since the deep-water waves do not reach the basin bottom. Force gauges were installed at the fairlead connection to measure the mooring line tensions.

Table 2
The scaled TLP wind turbine dimensions.

Dimension	Symbol	Model scale value
Foundation		
Floater diameter	D_{float}	500 mm
Floater height	h_{float}	200 mm
Floater thickness	t_{float}	5 mm
Transition piece diameter	D_{trans}	138 mm
Transition piece height	h_{trans}	300 mm
Transition piece thickness	t_{trans}	5 mm
Spoke root area	$w_{r.spoke} \cdot h_{r.spoke}$	100 mm·133 mm
Spoke tip area	$w_{t.spoke} \cdot h_{t.spoke}$	50 mm·42 mm
Spoke length	l_{spoke}	500 mm
Spoke thickness		5 mm
Mooring lines		
Fairlead position from root of spoke	l_f	450 mm
Mooring line diameter	D_{moor}	2.2 mm
Water depth	h	3000 mm
Hub		
Rotor diameter	D_{rotor}	2972 mm
Blade length	l_{blade}	1440 mm
Hub height o. MWL	h_{hub}	1870 mm
Tower		
Tower diameter	D_{tower}	80 mm
Tower height	h_{tower}	1682 mm
Tower thickness	t_{tower}	3 mm

An overview of the sensors used in the test campaign is provided in Fig. 3. More information about the calibration process as well as logging system and hardware setup can be found in Ref. [20].

All the signals, except those of the wind turbine motors, were analogue signals that were fed into a data acquisition system and logged with a frequency of 160 Hz. The signals coming from the two servo motors were digital signals and logged/controlled at 50 Hz.

Four different environmental conditions (ECs) were considered for the experimental studies: one for below rated wind speed, one for around rated wind speed, one for above the rated wind speed, and one for extreme wind condition. The selected conditions are shown in Table 3 and were a subset of the full environmental conditions introduced by Ref. [21]. However, due to a limitation on the maximum rotational speed of the wind generator fans, a maximum mean wind speed of 2.2 m/s at the turbine position could be achieved. Thus the scaled wind speed for EC6 and EC8 in Table 3 was reduced to 2.2 m/s.

4. Control

The implementation of control systems to the experimental model required the development of an interface between the two servo motors on the model turbine and the dynamic-link library (DLL) of the controller itself. The control implementation is a further development from the one utilized in Ref. [14]. The interface consisted of (1) a PC, hosting the user-interface which allowed for real time interaction with the controller, i.e. shutdown and logging data, (2) a National Instruments (NI) MyRIO connected to the two servo motors, running the controller code in real-time, and (3) two NI DAQs were used to simultaneously log signals from the equipment shown in Fig. 3. The latter allowed for synchronisation of the motion data with the operational parameters of the controller.

The implemented controller resembled the Basic DTU Wind Energy controller [18], although it only included the option of start-up and shutdowns along with control in the partial and full load region. Detailed mathematical formulations about the controller can be found in Ref. [18]. In addition, it should be noted that the main point of the tuning process in this paper was to match the scaled thrust curve rather than to match the scaled torque since the dynamic behaviors of the scaled floating wind turbine with different controllers were the most interesting phenomena to understand in this paper.

The objective for control in the partial load region is to maximize the generated power meaning that the turbine should operate at maximum value of the power coefficient, C_p. This is achieved by keeping the blade pitch setting and Tip Speed Ratio, $TSR = R\omega/v$ where R is the blade radius, ω is the rotational speed, and v is the wind speed. The partial controller thus adjusts the generator torque based on the rotational speed. This type of controller is well known and is called a $K - \omega$ controller where $0.0089 \, (\mathrm{Nm/(rad/s)}^2)$ of the optimum K value is used both for on- and offshore controller. The partial controller flowchart can be found in Fig. 4a.

The full load controller on the other hand has the objective to keep the rotational speed and generated power at their respective rated values. This is done by adjusting the collective pitch angle of the blades in response to errors in rotational speed based on a PI controller. The gains of the PI controller are scheduled based on changes in the pitch angle to compensate for variations in the operating point of the wind turbine. The flowchart of full load controller is shown in Fig. 4b. Full details of the controller is given in Ref. [18].

Two different closed-loop controllers were tested for the scaled floating wind turbine. The first controller was for a typical onshore turbine. It was tuned by pole-placement technique. The second one is for a floating wind turbine. The onshore controller is tuned such that control actions do not excite the natural frequencies of the structure where the integral and proportional gains were 0.1 (Nm/rad) and 0.28 (Nm/(rad/s)), respectively. For the floating wind turbine controller, the task is more challenging than the onshore wind turbine as the frequencies of the moving platform must be taken into account. The natural frequencies of the platform motion are very low therefore the tuning of the controller was adjusted in order to avoid instability where the integral and proportional gains were 0.02 (Nm/rad) and 0.07 (Nm/(rad/s)), respectively.

Instability for the platform motion, often referred to as 'negative damping' [23], can occur when the blade pitch controller is acting at one of the low frequency platform modes. As the platform moves forward, the rotor experiences a stronger apparent wind speed and increases the blade pitch. This reduces thrust and the forward motion is slightly amplified. A similar interaction occurs at the backward movement thus leading to resonant motion.

An important aspect of offshore control design is to ensure that the excitation frequencies do not coincide with the natural frequencies of the structure. Moreover, the wind turbine is also effected by the 1P and 3P frequencies from the rotating blades. All these factors have to be considered in the design phase of the offshore controller. If, however, the excitation forces coincide with the natural frequencies of the structure, resonance may occur with consequent increase in fatigue loads. The overview of frequencies is illustrated in Fig. 5 where an operational range of $\Omega = (53.02, 74.37)$ rpm, a wave climate with frequencies ranging between $f_{wave} = (0.63, 1.19)$ Hz and the natural frequencies determined in section 5.4 are shown.
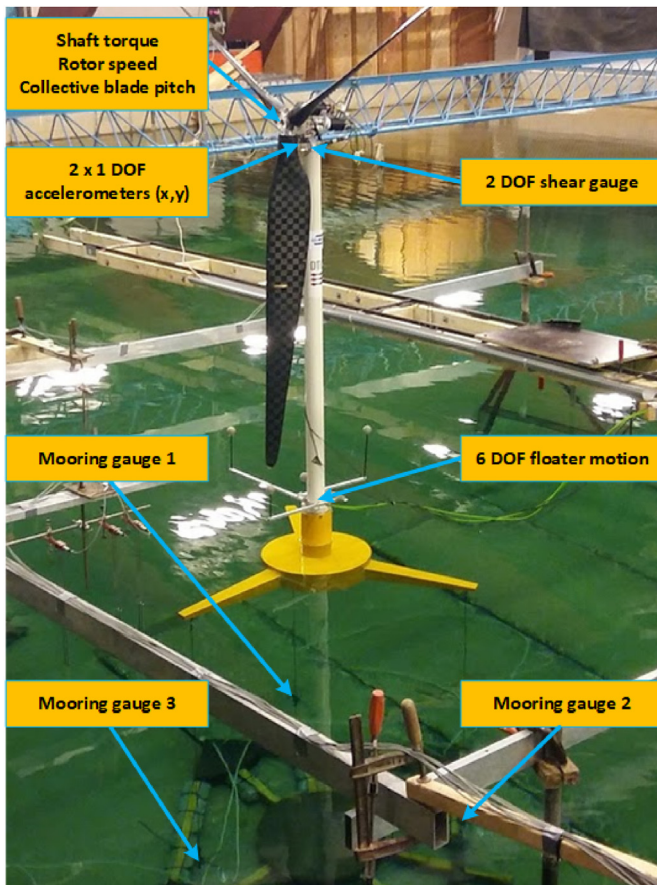

**Fig. 3.** The floating wind turbine instrumentation. DOF: degree of freedom.

Table 3
Table of target Environmental conditions (EC), taken from Ref. [21]. *: A wind speed of 2.2 m/s was used for sea state 6 & 8 due to wind generator limitations.

Environmental condition		EC3	EC5	EC6	EC8
H_s [m]	Full scale	3.30	4.16	6.18	10.0
	Model scale	0.055	0.069	0.103	0.167
T_p [s]	Full scale	6.50	7.30	8.90	12.20
	Model scale	0.84	0.94	1.15	1.58
$\overline{U}_{hub}$ [m/s]	Full scale	8.5	11.4	18.0	33
	Model scale	1.1	1.5	2.3*	4.3*
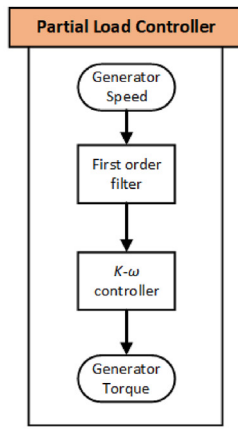
(a) partial load controller
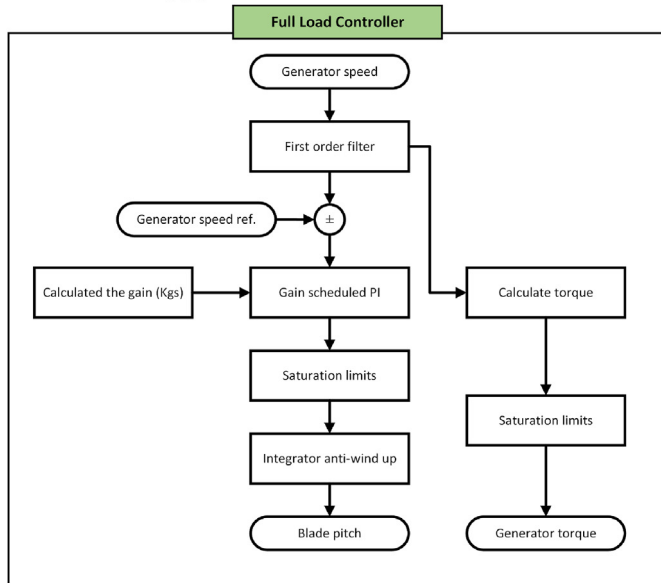
(b) full load controller

Fig. 4. Flowchart of the controller.

Fig. 5. Natural frequencies of the six degrees of freedom and the excitation frequencies from the rotational speed of the rotor and the waves.
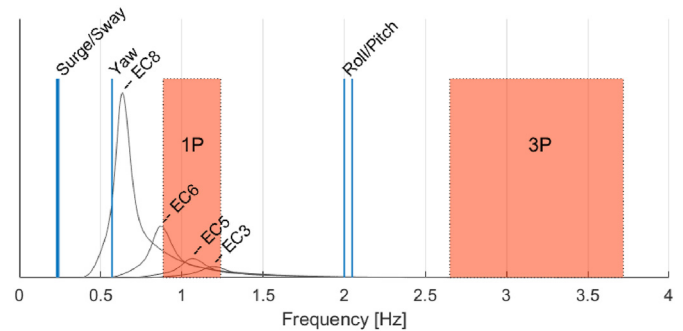
5. Climate validation

In this section we investigate to what extent the environmental conditions produced by the experimental setups such as wind generator, wave maker, wind turbine etc. resemble the target climates.

5.1. Wind climate

Prior to the production tests, the wind field generated from the six individual units was measured by sweeping four single component hot-wire air velocity probes across the frontal plane at the turbine equilibrium position, in which the rotor plane is a subset. A single probe was mounted on the wind generator to be present throughout the production tests.

A wooden frame with a steel rail on top was constructed, which would allow a cart with a pole to sweep across the wind field. The probes were then mounted on the pole and the cart was moved between five different positions across the plane for three different vertical positions of the probes. The wind speed was sampled for approximately 120 s in each position, corresponding to 15 min in full scale time.

The measurements were used for calibrating the commanded rotational speed of the wind generators and obtaining a correlation between the wind speed measured by the probe at the wind generator and the wind speed measured at the wind turbine position.

The sweep measurements were used to estimate the mean wind speed V and turbulence intensity TI in the rotor plane. The results for the three wind speeds of $V = (1.10, 1.47, 2.20)$ m/s are shown in Fig. 6. The rotor area is marked by a black circle and as it is evident that the measurements do not cover the entire rotor area, due to the cart having a certain height above the water, which is approximately 11% of the total rotor area. This means that in the azimuthal range $135 - 225$ deg the outer region of the blades will experience a drop in wind speed and an increased turbulence intensity. The results show that the wind field is relatively uniform and has low turbulence for the majority of the rotor area, with an overall mean turbulence intensity across wind speeds of about 3.5%. This means that the performance of the wind generators is overall satisfying. However it can be observed that the wind field in the lower left corner of the swept area is exposed to high turbulence and a significant low wind speed. This is likely due to a slight nonuniformity of the guiding vanes in the lower left wind generator, as stated in Refs. [16], resulting in the flow being directed to the center of the domain instead of making the flow uniform.
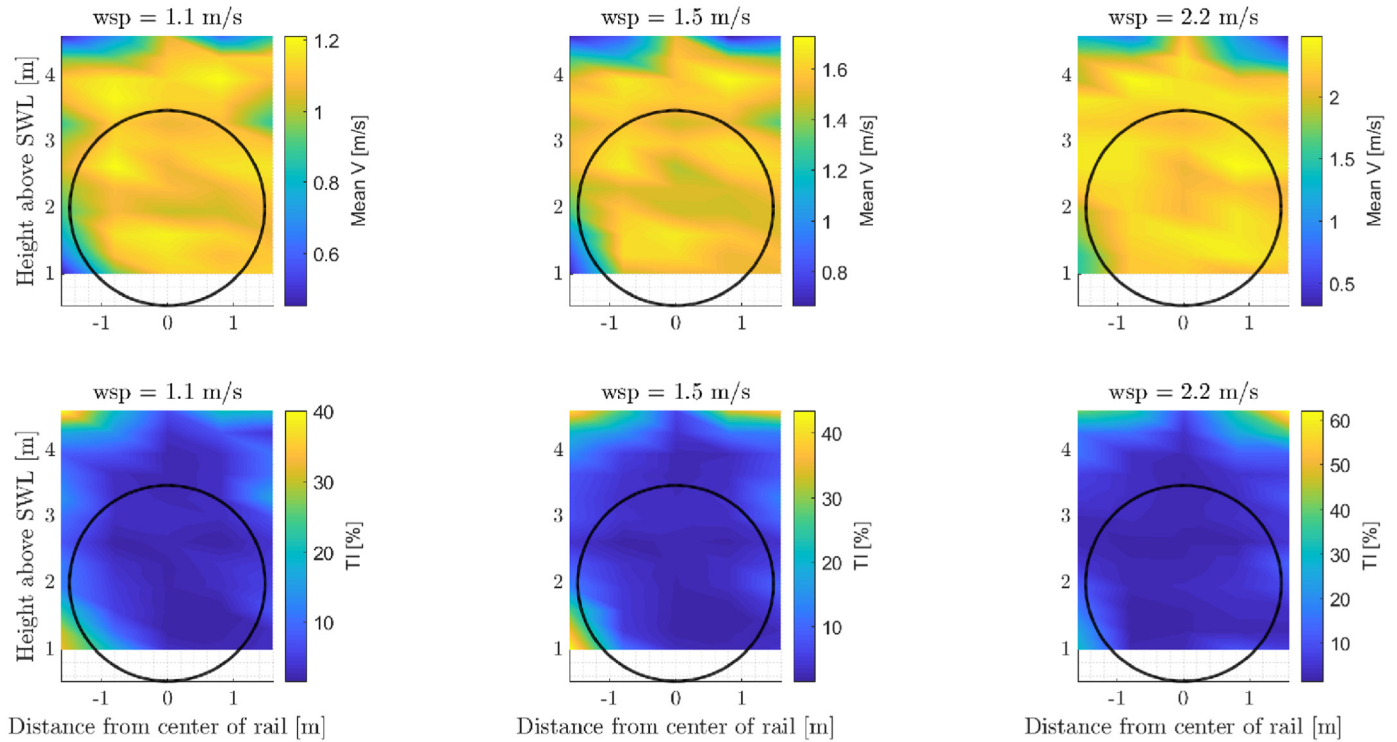
Fig. 6. Wind velocity fields and turbulence intensity field based on point measurements of wind speed averaged over 60 s.

5.2. Wave climate

Prior to mounting the floating wind turbine in the wave basin the wave fields were measured for the most severe sea state, namely EC8. A comparison was done based on wave gauge 8 and 9 shown in Fig. 2 and the measured wave elevation and period have been compared to the target Pierson-Moskowitz spectrum. Fig. 7 shows the measured spectrum of 5 realisations of each sea state compared with the target spectrum. A moving average filter was applied to the data. It is observed that the raw power spectral density (PSD) spectra compares well with the shape of the corresponding target spectrum. A comparison of H_s and T_p is shown in Table 4. EC8 shows a large difference in T_p of 17.7% between target and measured. However, Fig. 7 reveals a rather flat crest for the measured power-spectra, which introduce uncertainty in the determination of the measured T_p for EC8. In general, the match for the shape of the spectrum is good. The wave generation builds on

Table 4
Validation of irregular waves, H wave height and T wave period.

		EC3	EC5	EC6	EC8
H_s	Target	0.055	0.069	0.103	0.167
	Measured	0.057	0.072	0.102	0.165
	Difference [%]	3.6	4.3	0.97	1.2
T_p	Target	0.84	0.94	1.15	1.58
	Measured	0.83	0.90	1.12	1.30
	Difference [%]	1.2	4.2	2.6	17.7

linear wave theory and a clean Pierson Moskowitz spectrum. The observed local peaks other than the peak spectra period might be related to generation of second-order effects from the paddles of the wave maker. Since the theoretical spectra are based on linear theory it does not capture second-order effects.

5.3. Rotor thrust

In the downscaled test of offshore platforms, priority is traditionally given to the preservation of the Froude number, *Fr*. This means that the Reynolds number, *Re*, is not preserved, which represents a challenge when aerodynamics are involved. In our case, this means that for a given mean wind speed, *V*, a direct geometrically downscaled rotor will generally produce a different mean thrust force, *T*, than the reference DTU10MW wind turbine for the same rotor speed and blade pitch angle. The aerodynamic thrust is the most important aerodynamic element in the overall dynamics of a floating wind turbine, therefore it is desired to match the scaled thrust of the reference wind turbine for each wind speed. In the experimental setup, the rotor speed was always set to the downscaled reference value, and the match of the reference steady thrust curve was carried out by modifying the blade pitch settings for each wind speed until the mean thrust was equal to the target, see Fig. 8.
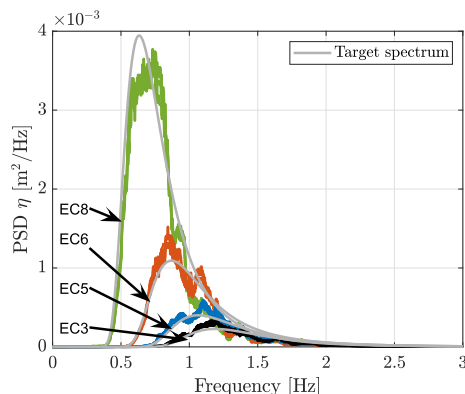

Fig. 7. Validation of irregular waves for the four environmental conditions (EC).

Since the rotor was designed with special low *Re* airfoils and a 75% increased chord, the steady thrust match was achieved with only minor adjustment of the blade pitch angle.

In Fig. 8 the initial blade pitch setting θ (bottom, red line) necessary to obtain the target thrust (blue line) is shown for the model and used as input to the controllers. In order to understand the sensitivity of the change of thrust over change of blade pitch, a sensitivity analysis was conducted for each determined blade pitch setting (red line) and the thrust curves for the sensitivity analysis correspond to deviations of ± 1 and 2 deg from θ (top, black and green lines: 1 and −2 deg and bottom, black and green lines: +1 and + 2 deg). However, for wind speed 1.7 m/s, the case where the blade pitch is θ − 2 produced aerodynamic torque beyond the limits of the wind turbine motor. Therefore, the sensitivity analysis for wind speeds 2.0 and 2.2 m/s was only carried out with for θ − 1, θ+ 1 and θ + 2 deg.

5.4. System free decay tests

Free decay tests of the entire floating wind turbine system including all structural properties were carried out by imposing an initial displacement to the structure in each of the degrees of freedom. By then releasing the structure the system characteristics can be determined, such as natural frequencies and the system damping. A line was attached to the structure, in order to impose a displacement in each of the degrees of freedom. In surge and sway, the line was attached to the floater at the waterline level. In roll and pitch, the line was attached some distance along the wind turbine tower. In yaw, the line was attached to the fairlead on the front spoke. Due to the high stiffness of the system in heave and the risk of slack tendons, it was not possible to get out satisfactory results for heave. The heave frequency is thus marked with brackets in Table 5 and the corresponding damping ratio could not be estimated. The measured natural frequencies and damping ratio are listed in Table 5, which are obtained based on the power spectra of the decay test. For each degree of freedom, three free decay tests were done in succession. Thus the values in Table 5 represent the average across these three decay tests. Initial displacements of

Table 5
Measured natural frequencies and damping ratios from experiments.

	Surge	Sway	Heave	Roll	Pitch	Yaw
EXPERIMENTS						
Frequency [Hz]	0.24	0.23	(9.83)	2.05	2.00	0.57
Damping ratio ζ [ ]	0.08	0.08	–	0.06	0.06	0.09

varying amplitudes were imposed in an attempt to capture both linear and nonlinear behaviour. However, due to the limitations of the method in applying the initial displacement for each degree of freedom as well as the expected nature of the system, it was not possible to completely isolate an initial displacement in the desired degree of freedom without inducing an initial displacement in other degrees of freedom. This was particularly seen for surge and pitch, and sway and roll, due to the strong couplings between these degrees of freedom.

5.5. Environmental conditions and turbine operational parameters

Based on the obtained validation results a complete table describing the environmental conditions (EC) and turbine operational parameters are provided in Table 6. It shows the wave height, H_s, period, T_s, the wind speed at hub height, V_{hub}, and the corresponding operational conditions; rotor speed, Ω, and blade pitch, θ_p, for the open loop controller (also noted "fixed"). EC8 is meant to represent storm conditions with a parked turbine. However it was decided to have the turbine active in EC8, as the wind speed could not exceed 2.2 m/s due to the limitations of the wind generators.

6. Experimental results
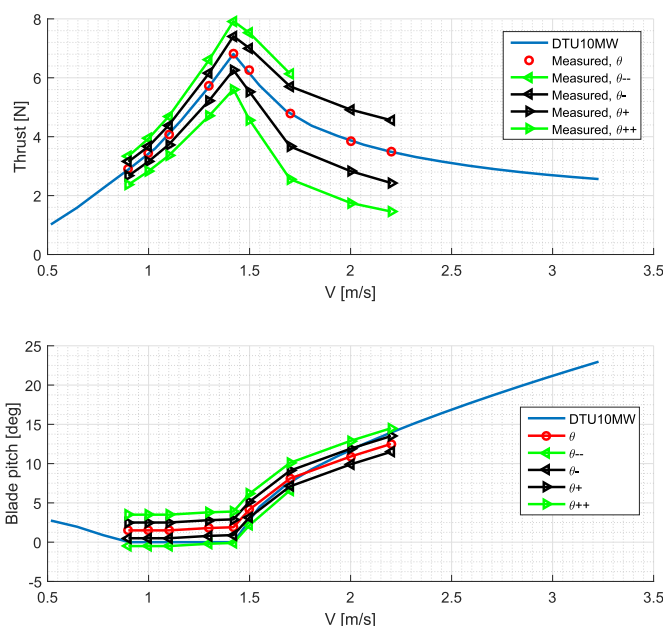
6.1. Effect of wind and wave misalignment

The irregular sea states consist of several wave groups with different heights and lengths. Hence they are best suited to represent real sea states. However, due to the random nature of irregular waves, the comparison of responses in time series becomes impractical. Therefore the exceedance probability P is introduced.

For each signal and for each environmental state, the peaks were identified and stored based on a wave elevation zero down-crossing [24]. The time series of the incident wave elevation is divided into individual waves, where each wave is defined between two zero down-crossings of the free surface elevation. The maximum values of the specific signal are then determined within each time range defined by the individual waves and stored. The peaks X are sorted from minimum to maximum and assigned with an index i to compute the exceedance probability based on the index and the total number of peaks N. This approach ensures that only one independent response peak per wave is registered [21] and the exceedance probability P can be defined as:

Fig. 8. Rotor thrust tests for the wind turbine. Note that $\theta_\pm$ corresponds to a 1 or 2 deg deviation from the desired pitch angle setting.
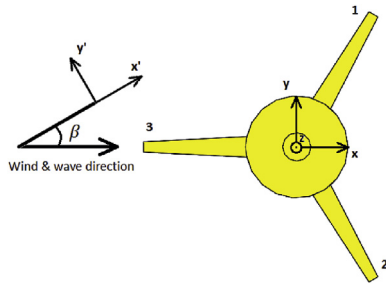
Table 6
Environmental conditions and turbine operational parameters for the experiments. A wind speed of 2.2 m/s was used for sea state 6 & 8 due to wind generator limitations.

	Environmental conditions			Turbine operational parameters	
	H_s [m]	T_s [s]	V_{hub} [m/s]	θ_p [deg]	Ω [rpm]
EC3	0.055	0.84	1.1	1.50	53.02
EC5	0.069	0.94	1.5	4.17	72.11
EC6	0.103	1.15	2.2	12.50	74.37
EC8	0.167	1.58	2.2	12.50	74.37

Fig. 9. Wave coordinate system and global floater coordinate system.

$$P = p(X \geq x_i) = 1 - \frac{i}{N+1} \tag{1}$$

All the misaligned irregular wave tests were conducted with a wave heading of $\beta = 30°$ as defined in Fig. 9. When dealing with misaligned waves, the response is typically projected into the wave coordinate system, see Fig. 9. This allows for a more appropriate comparison of the effect of misalignment on the different degrees of freedom, hence the surge, sway, roll, and pitch ($\xi_1, \xi_2, \xi_4, \xi_5$) in cases with misalignment were projected into the direction of the

wave propagation, while heave and yaw (ξ_3 and ξ_6) remained unchanged. It should also be noted that the nacelle accelerations were also projected into the wave coordinate system.

Since the impact from the aerodynamic force is largest at rated conditions (EC5), it is chosen for the misalignment analysis. Furthermore the closed-loop controller tuned for the offshore floating configuration was used for the cases with wind. The response in the six degrees of freedom for tests with and without wind had their corresponding mean subtracted from the signals in order to highlight the differences in the dynamics.

This means that four cases will be presented in each figure; aligned and misaligned waves with and without wind. Furthermore the power density spectra of the responses will be presented together with the exceedance probability curves.

The effect of misalignment and wind on surge motion and nacelle fore-aft and side-side accelerations for EC5 are shown in Fig. 10. The surge motion in aligned waves and without wind (blue) shows as expected the largest response and the effect of the aerodynamic damping can be seen on the exceedance probability plot, as the response with wind included (red), is smaller. However, the damping effect is minor for the misaligned waves case (yellow and purple), as only a component of the wind will affect the surge. Thus the aerodynamic damping is strongest on the surge motion for unidirectional conditions. If the signals did not have their mean
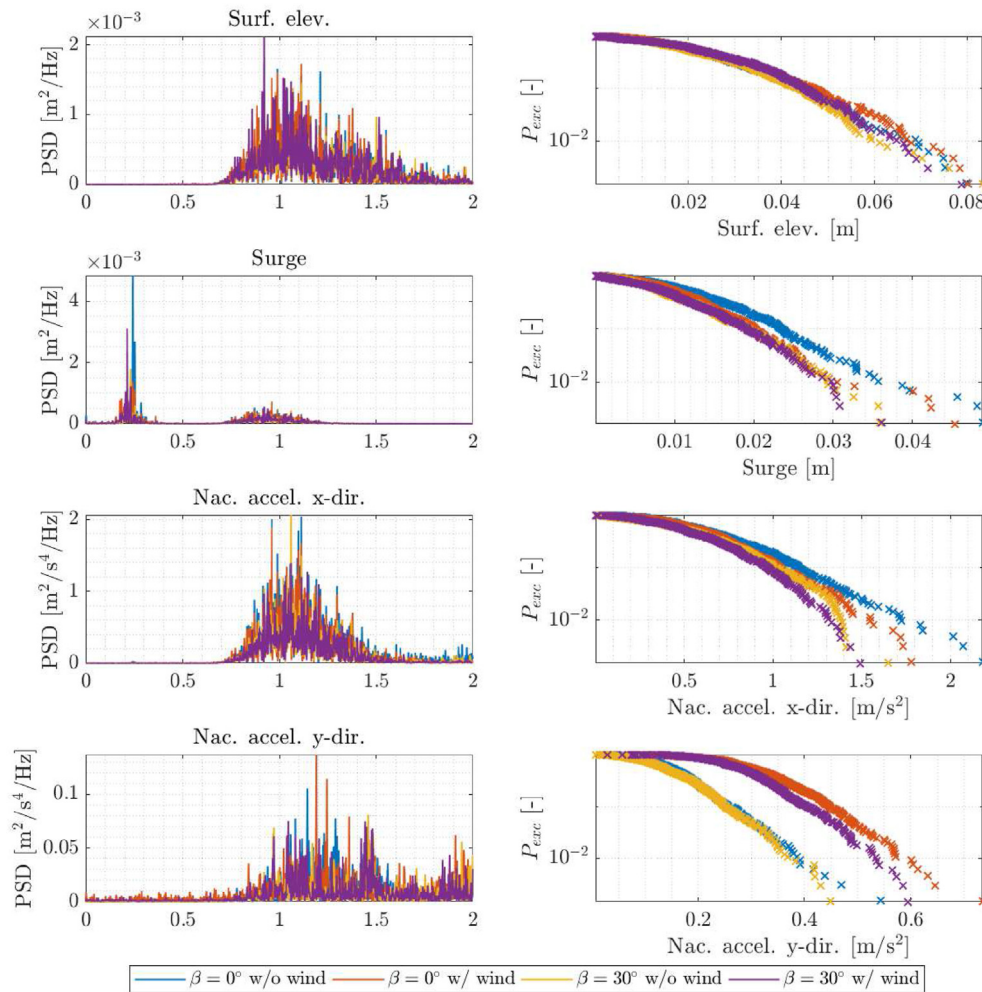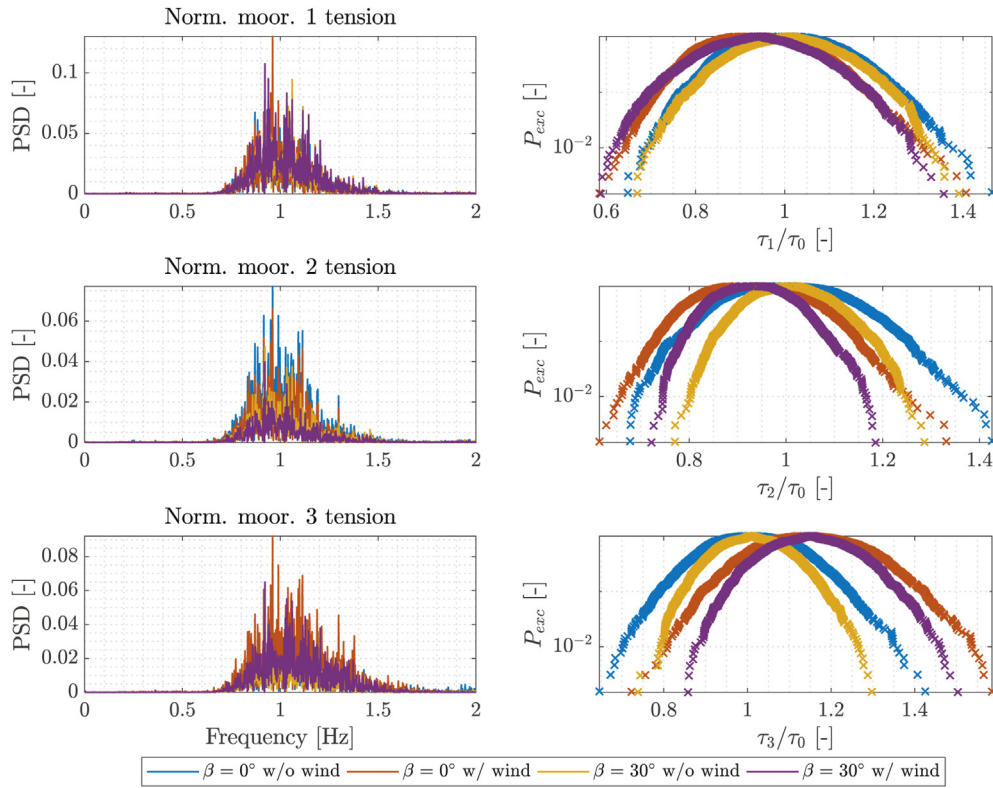

Fig. 10. The comparison of floater surge response and nacelle accelerations in irregular waves with wave heading $\beta = 0°$ and $\beta = 30°$ with and without wind for EC5. Mean values have been subtracted and the signals have been projected into the direction of the wave propagation. The x,y-directions refer to fore-aft and side-side accelerations in the wave coordinate system, see Fig. 9.

Fig. 11. Normalised mooring line tensions in irregular waves with wave heading $\beta = 0°$ and $\beta = 30°$ with and without wind for EC5. Mean values have not been subtracted, but the tensions are normalised with the equilibrium state τ_0, thus the tensions in calm water and without wind. The labelling of τ_i refers to Fig. 9.
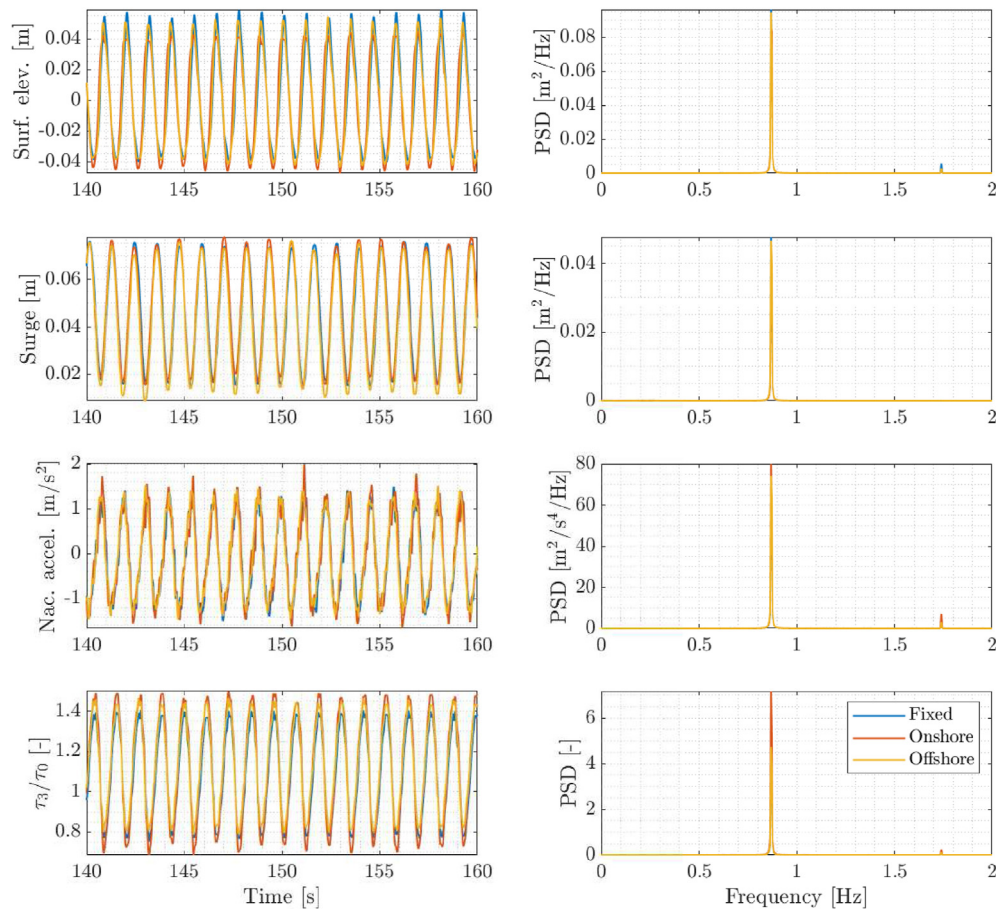
Fig. 12. Surge, nacelle fore-aft acceleration and normalised front mooring line tension for regular waves in EC6 with different controllers.
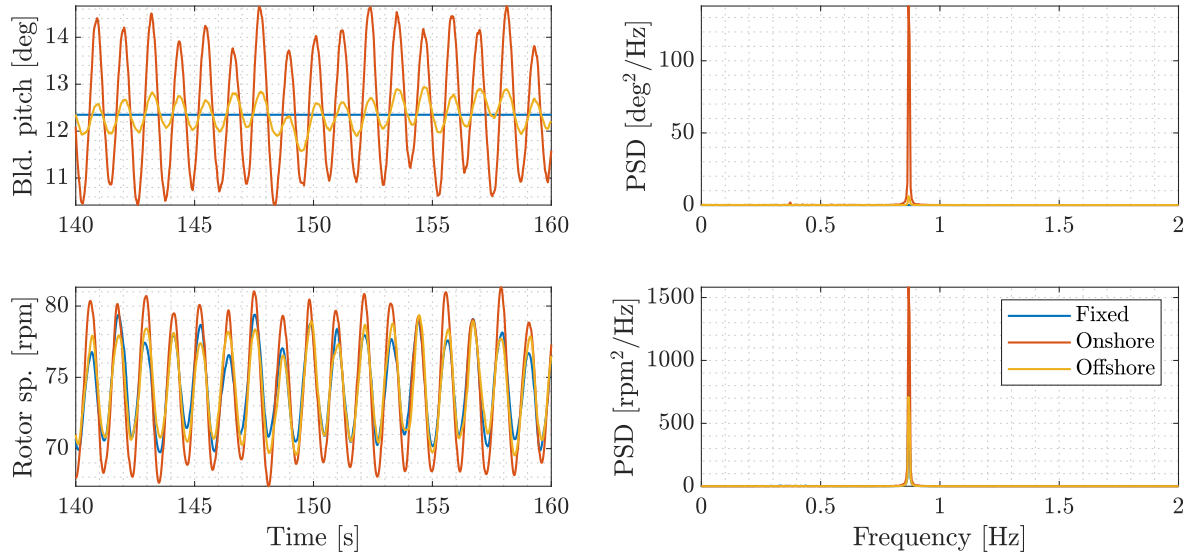
Fig. 13. Turbine operational data (blade pitch and rotational speed) for regular waves in EC6 with different controllers.
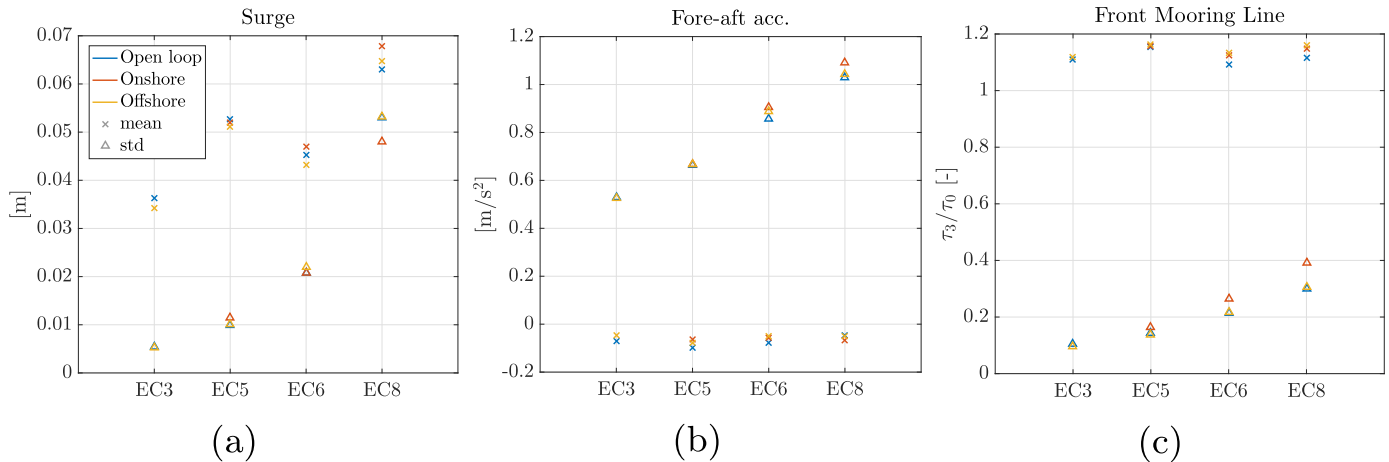

Fig. 14. Mean and standard deviation for (a) Surge, (b) Nacelle fore-aft acceleration, (c) Normalised tension in the front mooring line.

value subtracted, a permanent offset for the wind and wave misaligned case would be expected, since the wind will induce a component in the negative y'-direction, see Fig. 9.

The same can be observed for the nacelle accelerations exceedance probability plots in the x-direction, which were also transformed into the wave coordinate system. Here the cases without wind also lie above the cases with wind. It can also observed that introducing wind to the system will increase the out-of-plane acceleration (y-direction).

Fig. 11 presents the normalised tension in the three mooring lines at rated wind speed. It can be observed that, for the tension in mooring line 3 (see Fig. 9), the wind-induced mean moment adds a permanent positive increase in the mean value for both aligned and misaligned conditions. The opposite picture is present for mooring line 1 and 2.

Further, the tension in mooring line 1 appears to be unaffected by misaligned waves or wind, which could be due to the wave direction in x' achieving only an offset of 30° offset with spoke number 1. Furthermore the overall magnitude of the loads in the two other mooring lines decrease slightly when misaligned waves are applied.

6.2. Controller performance

6.2.1. Regular waves

The three controllers are compared with respect to their impact on the system response and they will in following be referred to as *offshore*, *onshore* and *fixed* which refer to the closed-loop controller tuned for offshore floating configuration, the closed-loop controller tuned for onshore and the open-loop controller with fixed rotational speed and fixed blade pitch, respectively.

In Fig. 12 the surge motion, nacelle fore-aft acceleration and front mooring line tension are presented together with their corresponding power spectra for environmental conditions. The analysis is done for environmental conditions above rated wind speed conditions, in this case EC6, to better isolate the effects from the full-load controller. It is observed that the surge motion, nacelle fore-aft acceleration and front mooring line tension are dominated by response at the wave frequency at 0.87 Hz. Furthermore minor low-frequency response is visible for particularly the onshore controller in the time series, oscillating with the natural frequency of surge, 0.24 Hz. However this contribution, compared to the wave excitation, is significantly lower, and thus not visible in the PSD
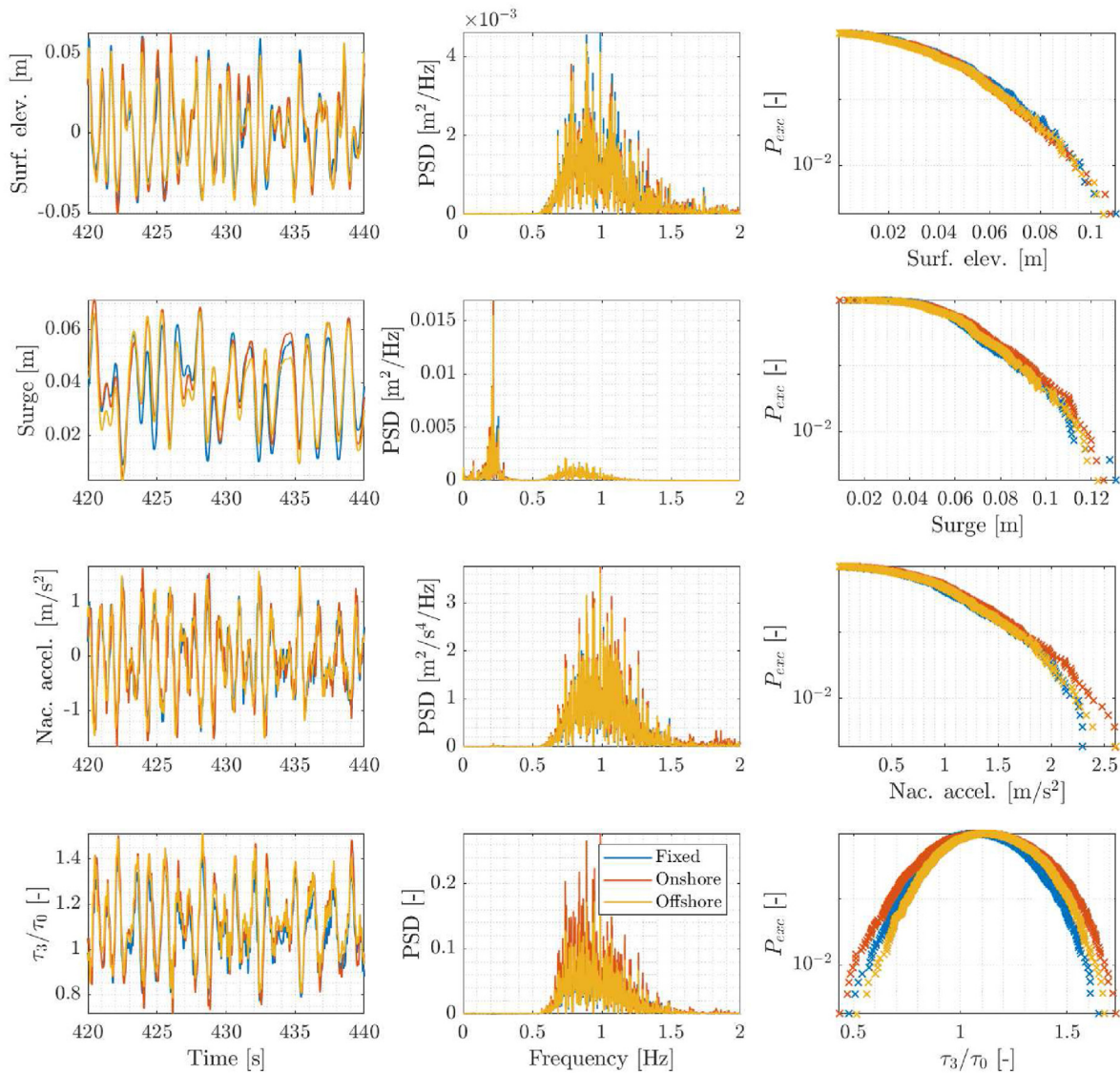
Fig. 15. Surge response of the floater platform, nacelle fore-aft acceleration and normalised front mooring line tension in irregular waves with three different controllers for EC6.

plot. Only by observing the PSD in logarithmic scale, a minor contribution can be seen. The higher surge motion for the onshore controller compared to the offshore and open loop controller, will result in higher mooring line tensions. The front mooring line tension can be observed to be up to 3% higher for the onshore controller compared to the offshore controller and 6% higher than the open loop controller. It is observed that all three controllers achieve approximately the same nacelle accelerations and with dominating response at the wave frequency. However the onshore controller is also excited slightly at the second wave peak frequency, i.e. $T_p/2$, and tend to have higher extreme values.

Fig. 13 shows the operational data of the turbine, blade pitch and rotational speed with corresponding power spectra, for the same environmental conditions above rated wind speed (EC6). As expected, rapid and large-amplitude blade pitch response is seen for the onshore controller for rated conditions, whereas the offshore controller is more slow, thus much less aggressive. This emphasizes that the offshore controller is tuned to handle motion due to waves rather than control due to wind. The extreme blade pitching of the onshore controller also affects the rotational speed and causes

higher magnitude of oscillations. Further it is seen, that the rotational speed of the fixed controller configuration is not constant. This is due to the servomotor on the shaft not being able to supply the needed torque to stay at the desired rotational speed value.

In addition in Fig. 14 the mean and standard deviation for the regular wave cases are presented with respect to surge motion, nacelle fore-aft acceleration and front mooring line tension. The reader should recall that the wind is the same for EC6 and EC8 due to limitations of the wind generators and only the waves are larger for EC8.

The mean surge response has a local maximum at rated wind speed (EC5) due to the trend of the thrust curve, but then as the environmental conditions become more severe (EC8), the mean is increased. This is due to the increased non-linear effects, which are more severe for larger wave amplitudes, imposing a mean drift force, a trend that can be seen in both the surge response and the mooring tensions. Similar tendencies are observed for the tensions in the front mooring line. Furthermore it is observed that the standard deviation of the tensions for the onshore controller are increasing rapidly for higher environmental states compared to the
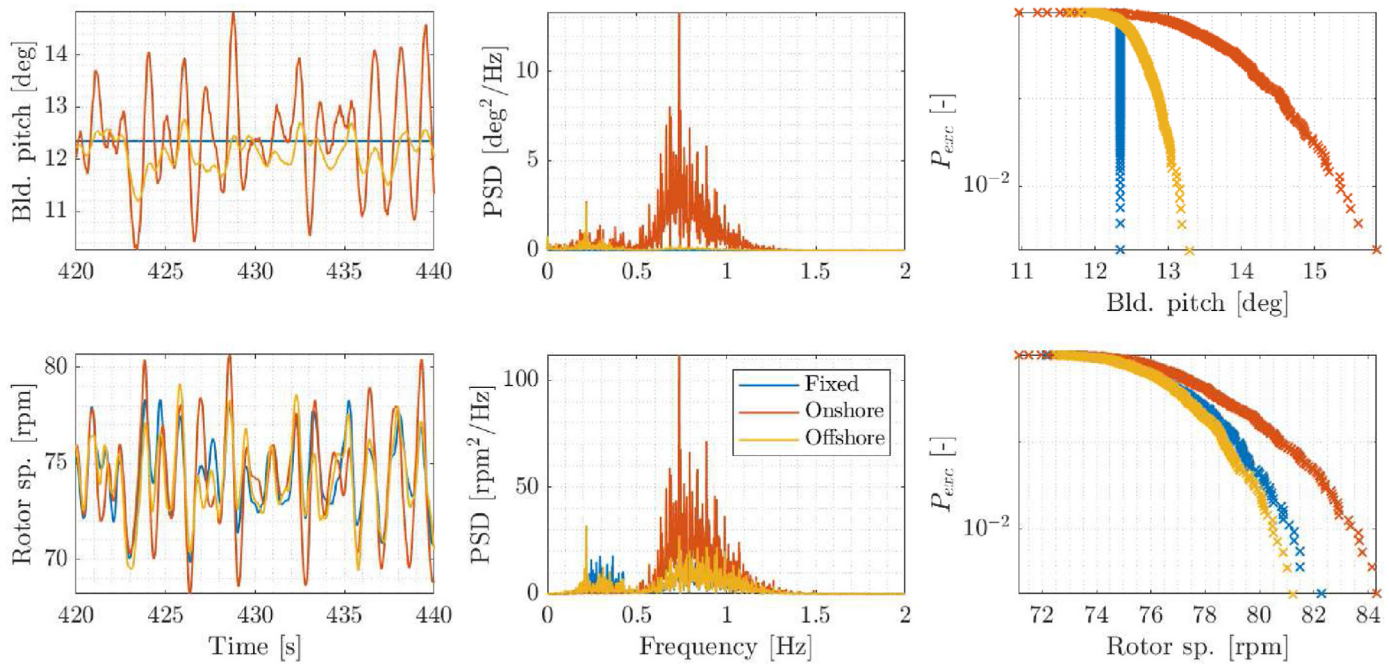
Fig. 16. Turbine operational data (blade pitch and rotational speed) in irregular waves with three different controllers for EC6.

two other controllers. This is due to the negative aerodynamic damping for this controller.

It can be observed that the means of the nacelle fore-aft acceleration are close to zero for all environmental states, which is to be expected. The slight offset from zero is due to the small wind-induced mean pitch moment that introduces a gravitational component. Since a horizontal gravity component will be captured by the accelerometer and the fact that the center of mass for the Rotor Nacelle Assembly (RNA) is located slightly upwind, there is an offset in the negative direction. Further the standard deviation shows, an increase with increasing sea state, but more rapidly for the onshore controller.

6.2.2. Irregular waves

The three different control systems are now analysed in aligned irregular waves. Comparison of the controllers will be carried out based on the response above rated conditions, EC6.

Fig. 15 shows the influence of the three controllers on the surge motion, nacelle fore-aft acceleration and front mooring line tension (normalised). In general, the offshore controller performs best as it keeps the dynamic surge response and the front mooring line tension low. Overall the performance of the onshore controller results in larger surge response than the offshore controller, thus leading to larger front mooring line tensions. It is seen that the surge motion for the three controllers are dominated by a combination of excitations of the surge natural frequency and at the wave frequency range. The nacelle acceleration and front mooring line tension are on the other hand only dominated by the waves.

Corresponding blade pitch and rotational speed are presented in Fig. 16. Note that for the closed-loop fixed control, a specific blade pitch angle is kept constant at 12.50°, hence a constant vertical line is seen in the exceedance probability plot. The aggressiveness of the onshore controller can be seen easily, as it pitches the blades more than the offshore controller. Looking at 90% percentiles of the blade pitch angle, the offshore controller is 12.9°, whereas the onshore is at 14.6°. Further it is seen from the PSD that the blade pitch is dominated by the waves for the onshore controller, whereas excitations at the surge natural frequency dominates the offshore controller. The effect

of the aggressive pitching of the blades for the onshore controller causes likewise the rotational speed to achieve the highest values of all the three controllers. From the PSD it is clear that the rotational speed of the onshore controller is purely dominated by the waves, whereas it is combination of the waves and excitations of the surge natural frequency for the two other controllers.

6.2.3. Extreme focused wave groups

Extreme wave episodes can be represented by the use of focused wave groups, which have similarities to the irregular wave type, as they are composed of a sum of individual waves over a range of frequencies. However, the focused wave groups have a chosen phase between the individual waves, resulting in a constructive merge at a single location x_0 and time t_0, namely the focus point. The surface elevation $\eta(x, t)$ for a group of focused waves can be described by:

$$\eta(x, t) = \sum_{i=1}^{N} a_i \cos(\omega_i(t - t_0) - k_i(x - x_0)) \qquad (2)$$

where $a_i = S_\eta(f_i)\Delta f$ is the amplitude, $\omega_i = 2\pi f_i$ is the frequency and k_i is the wave number of the individual waves. The maximum wave height, H_{max}, for the focused wave signals is chosen as the 3-h value according to a Rayleigh distribution for linear waves, $H_{max} = 1.86H_s$ [25].

The analysis presents the impact of a single large wave group on the structure giving insight into the extreme wave effects. The extreme response of the structure is investigated for the three controllers. In order to analyse the contributions from the wave frequency range and system natural frequencies, all measurements are presented with a time series in the left column and with corresponding power spectrum in the right column in Figs. 17 and 18. Since only a single wave group is analysed, the probability of exceedance is not relevant here, and for this reason only the time series and corresponding PSD are shown. As in the previous control sections, the comparison of the controllers is carried out based on the response above rated conditions, EC6.

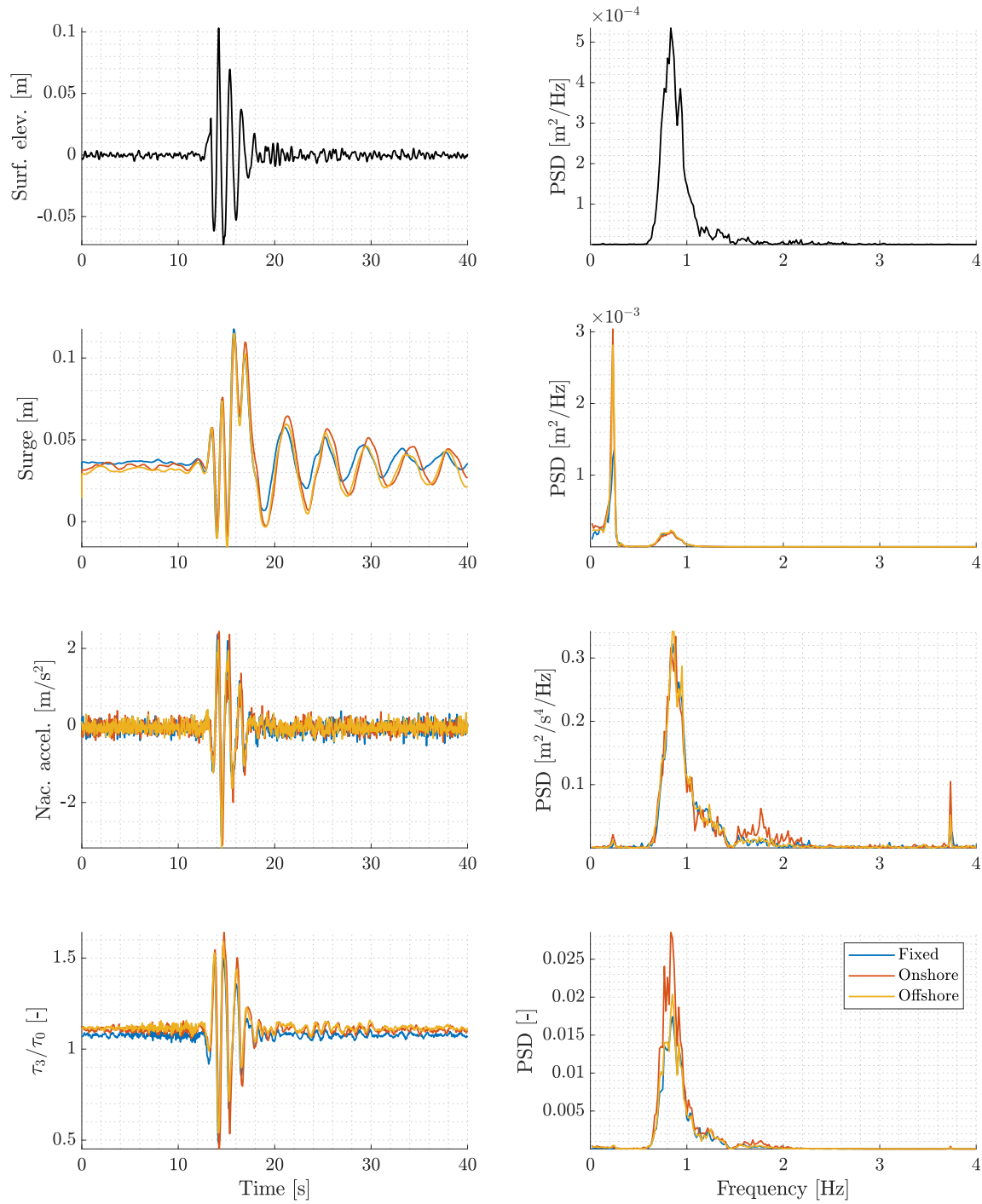Fig. 17 presents the wave elevation corresponding to the

Fig. 17. Surge response, nacelle fore-aft acceleration and normalised front mooring line tension for three different controllers in EC6 focused waves.

environmental state EC6 focused wave climate together with the surge motion, nacelle fore-aft acceleration and normalised front mooring tension.

As it can be seen, the impulsive excitation force from the focused wave group imposes a surge response of 0.12 m after the wave crest. It can be observed that the impact of the focused wave group causes a short sudden offset in the mean displacement of the surge motion, which is a nonlinear effect. After the focused wave group has passed, the structure decays back to equilibrium. This is why the surge motion is dominated by its own natural frequency of 0.24 Hz

and with only minor energy at the wave frequency range. This is observed for all three controller configurations, but the damping (and thus energy level) of the decays are different. The fixed controller shows the strongest damping of the three configuration, which is due to the blade pitch is kept constant according to the mean wind speed, resulting in the largest positive damping. The onshore controller is less damped compared to the offshore controller, due to the fact that the natural frequency of offshore controller is reduced and thus less excitations at the surge natural frequency occur. This agrees well with onshore controller being
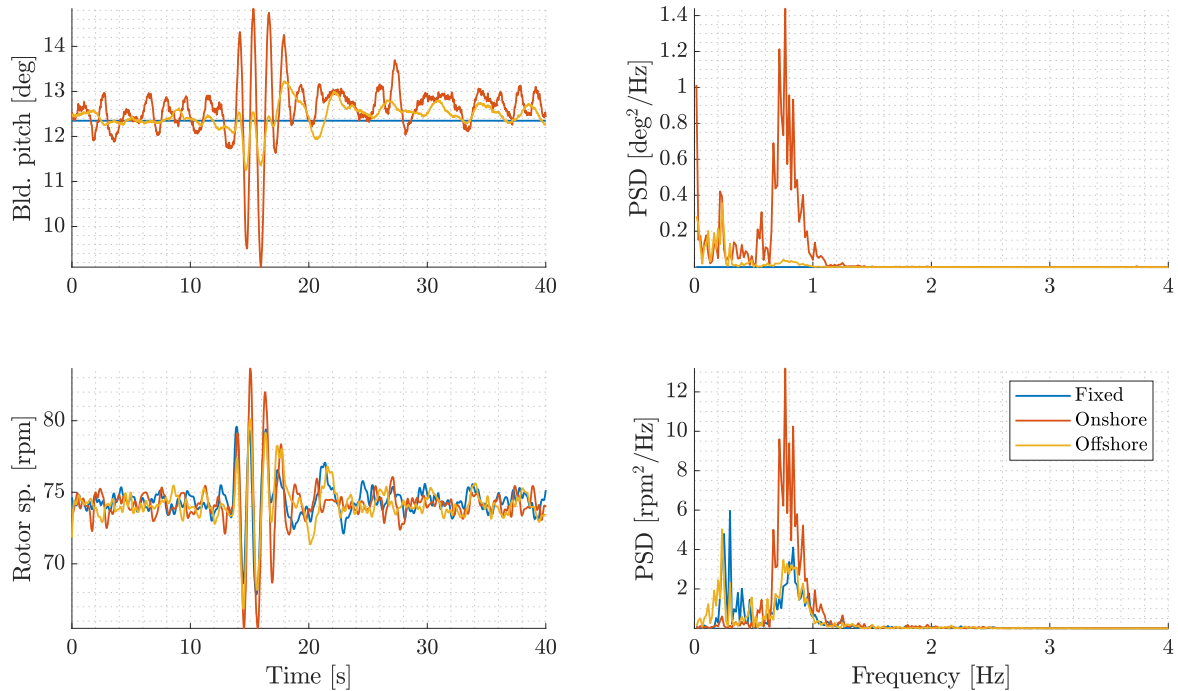
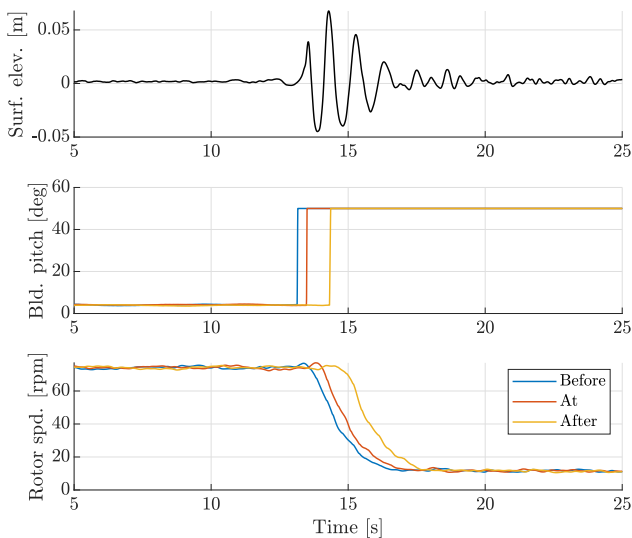Fig. 18. Turbine blade pitch and rotational speed for three different controllers in EC6 focused waves.

Fig. 19. Wave elevation η, blade pitch angle θ_p and rotational speed Ω for the shutdown cases of the offshore controller in EC5 focused wave climate.

able to excite instabilities when the controller is acting on one of the low frequency platform modes, as described in Section 4, leading to high surge response.

The nacelle acceleration responses for all three controllers are similar. From the corresponding power spectra it can be observed, that they are all dominated by the waves and have approximately the same level of energy at the wave frequency range. However, it is also clear that the motion of the onshore controller is further excited by the super harmonics at twice the wave peak frequency. Furthermore the 3P excitations at 3.89 Hz are significantly larger for the onshore compared to the other two and as for the surge motion lowest for the fixed configuration. This can be linked to the low level of damping for this controller.

Looking at the front mooring line tension, the onshore controller experiences the largest loads compared to the other two configurations. The maximum tension amplitude is increased with 3% compared to the offshore controller and 9% to the fixed configuration. It should also be pointed out that the mooring line tensions are dominated by the wave forcing and no significant excitations of the response natural frequencies are seen.

In Fig. 18 the corresponding blade pitch and rotational speed of the turbine are presented. From the blade pitch the source of the increased mooring line tensions for the onshore can easily be seen, i.e. the severe reaction to the wind and waves. The blade pitch response for the onshore controller is dominated by the waves and the wind (shown by the peak furthest to the left), whereas the offshore controller is dominated by the surge natural frequency (0.24 Hz) and only very slightly excited by the waves.

Controlwise the results are very similar to the irregular wave case, only with enhanced excitations at the surge natural frequency, due to the decay after the impact of the focused wave group.

6.2.4. Turbine shutdown

The impact of shutdown on the motion of the structure is investigated and the best way to see the impact is by using the extreme events, ie. the focused wave groups. The analysis is conducted with the offshore controller configuration, and in the environmental case where the effect of wind is at maximum, hence rated wind speed, EC5. The shutdown of the controller was done manually and the aim was to have a shutdown at three different moments: i) before the highest crest of the focused wave group hit the structure, ii) at the very instant the wave crest breaks at the turbine position and iii) right after. In the following figures the labels *Before*, *At* and *After* refer to where the shutdown was executed relative to the wave peak. The procedure of the shutdown was so that the pitch was ramped from the instantaneous value to maximum pitch of 50 deg with a rate of 15 deg/s (compared to the normal operation rate of 10 deg/s) and the generator torque set to zero.

Fig. 19 presents the blade pitch angle θ_p and rotational speed Ω
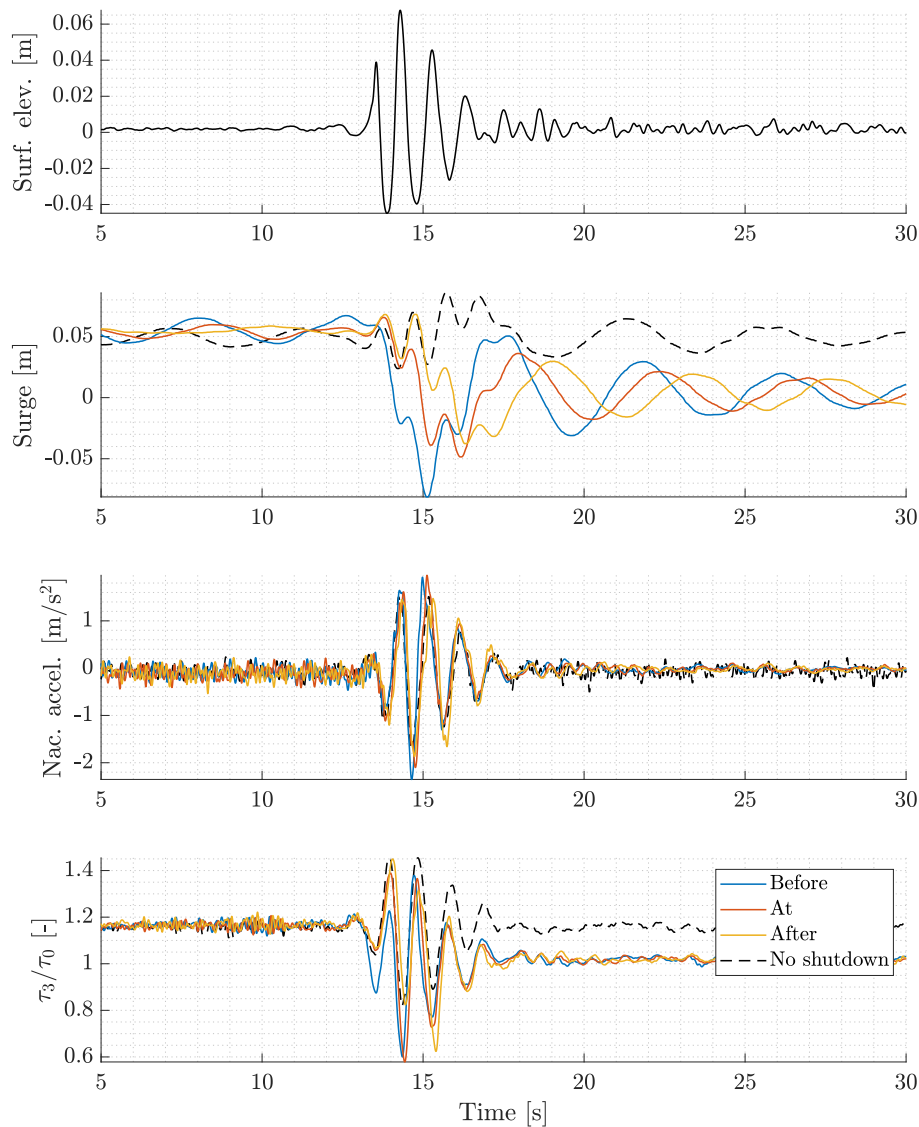
Fig. 20. Surge response, nacelle fore-aft acceleration and normalised front mooring line tension for the shutdown cases of the offshore controller in EC5 focused wave climate.

of the turbine for the shutdown cases. Due to the manual shutdown procedure it was very challenging to shutdown the turbine at the exact point of wave impact on the structure. It is evident from the blade pitch angle signal that the shutdown case at the point where the wave hit the turbine is actually a bit before. However, the test is still considered in the analysis. It is seen from the rotational speed that the rotor does not reach 0 rpm after a shutdown. This is due to the maximum pitch angle being 50 deg and the fact that the generator torgue is zero, causing an idle state of the turbine with a rotational speed of about 12 rpm in EC5.

The corresponding motion response, in terms of surge motion, nacelle fore-aft acceleration and normalised front mooring line tension, can be seen for the three shutdown cases in Fig. 20. Furthermore, the black dashed lines in the plots represent the focused wave test where no shutdown was executed, but with the same controller. The highest surge response of nearly − 0.1 m is achieved in the case where the turbine is shutdown before the wave impact. This can be explained by the incoming trough forcing the turbine upwind and in the moment the shutdown appears, the loss

of the thrust force acting on the rotor will cause the structure to experience a restoring force in the negative x-direction, resulting in an even greater surge displacement. The opposite effect is seen when the turbine is shutdown right after the break of the crest, where the surge displacement is damped. Releasing the thrust force will generate a high pitching moment and for the shutdowns before the wave impact, two major negative peaks can be observed, hence one from the shutdown and one from the wave peak. Only a slight increase in nacelle fore-aft acceleration can be observed, but the front mooring line, that is governed by the pitching motion, experiences very low tension when shutdown occur close to $\tau_3/\tau_0 = 0.5$. Approximately 33% decrease of the tension can be observed for shutdown before the wave impact compared to the case, where no shutdown is executed.

7. Conclusion

The present work detailed the experimental testing of a Tension Leg Platform (TLP) substructure designed by the Korea Institute of

Energy Research (KIER) and the pitch-regulated scaled 1/60 DTU 10 MW reference wind turbine. The investigation included the response in regular waves, irregular waves, focused waves and a low turbulent wind field tested with different turbine controllers.

Before the wave tests, the aerodynamic performance of the fixed model scaled turbine was successfully tuned to match the down-scaled steady thrust curve of the 10 MW reference turbine. The turbine was then mounted on the floater and free decay tests in still water provided insight of the structural natural frequencies and damping ratios.

Detailed analyses of the dynamic response of the three control configurations were carried out and it was observed that sensitivity of the onshore controller resulted in high oscillations in blade pitch, yielding an increased response in surge for all wave types. It was also observed that the surge motion governed the mooring line tensions, thus the onshore controller yielded the highest tensions in the front mooring line. Further the shutdown cases of the offshore controller led to larger surge displacement when the shutdown was initialized right before the wave impact. This was explained in terms of aerodynamic damping.

The present analysis demonstrates the potential of physical model testing, as part of the development of a new concepts. However physical model testing are also a crucial part of validating numerical models, which will be investigated as future work. This plays an important role in the design phase of floating support structures, both adding reliability to the design tools and confidence to the sector of floating wind turbines, and further ultimately pushing the offshore industry forward, thus bringing down the cost of offshore wind energy.

Author contribution statement

1. Freddy J. Madsen: Methodology, Writing original draft preparation, visualization, Investigation, Formal analysis, Data Curation.
2. Thomas R. L. Nielsen: Methodology, Writing original draft preparation, visualization, Investigation, Formal analysis, Data Curation.
3. Taeseong Kim: Supervision, Methodology, Conceptualization, Investigation, Writing, Reviewing and Editing, Project administration, Funding acquisition.
4. Henrik Bredmose: Supervision, Methodology, Investigation, Writing, Reviewing and Editing.
5. Antonio M. Pegalajar-Jurado: Investigation, Writing, Reviewing and Editing, Data Curation.
6. Robert F. Mikkelsen: Methodology, Investigation, Resource.
7. Anders K. Lomholt: Investigation, Data Curation.
8. Michael Borg: Investigation, Writing, Reviewing and Editing, Data Curation.
9. Mahmood Mirzaei: Methodology, Investigation, Writing, Reviewing and Editing, Data Curation.
10. Pyungho Shin: Investigation, Data Curation.

Declaration of competing interest

The authors declare that they have no known competing financial interests or personal relationships that could have appeared to influence the work reported in this paper.

Acknowledgements

References

[1] The European Parliament, The Council Of The European Union, Directive 2009/28/EC of the European parliament and of the council of 23 April 2009 on the promotion of the use of energy from renewable sources and amending and subsequently repealing Directives 2001/77/EC and 2003/30/EC, Off. J. Eur. Union 140 (2009) 16—62.
[2] The Council Of The European Union, A policy framework for climate and energy in the period from 2020 to 2030, ENVE-V-047, 108th Plenary Session, 6, 7 and 8 October 2014, 2014.
[3] Wind Europe, Offshore Wind in Europe - Key Trends and Statistics 2018, 2019.
[4] Catapult Offshore Renewable Energy, Floating Wind: Technology Assessment, 2015.
[5] R. James, M. Costa-Ros, Floating Offshore Wind: Market and Technology Review, 2015.
[6] R. James, W. Weng, C. Spradbery, J. Jones, D. Matha, A. Mitzlaff, R.V. Ahilan, M. Frampton, M. Lopes, Floating Wind Joint Industry Project - Phase I Summery Report, CARBON TRUST, 2018. May 2018.
[7] J. Jonkman, T. Larsen, A. Hansen, T. Nygaard, K. Maus, M. Karimirad, Z. Gao, T. Moan, I. Fylling, J. Nichols, M. Kohlmeier, J. Pascual Vergara, D. Merino, W. Shi, H. Park, Offshore code comparison collaboration within IEA wind task 23: phase IV results regarding floating wind turbine modeling, in: European Wind Energy Conference (EWEC2010). Warsaw, Poland, 2010. April 20-23.
[8] A. Robertson, J. Jonkman, F. Vorpahl, W. Popko, J. Qvist, L. Frøyd, X. Chen, J. Azcona, E. Uzunoglu, C. Guedes Soares, C. Luan, H. Yutong, F. Pengcheng, A. Yde, T. Larsen, J. Nichols, R. Buils, L. Lei, T.A. Nygaard, D. Manolas, A. Heege, S.R. Vatne, H. Ormberg, T. Duarte, C. Godreau, H.F. Hansen, A.W. Nielsen, H. Riber, C. Le Cunff, F. Beyer, A. Yamaguchi, K.J. Jung, H. Shin, W. Shi, H. Park, M. Alves, M. Guérinel, Offshore code comparison collaboration continuation within IEA wind task 30: PhaseII results regarding semisubmersible wind system, in: 33rd International Conference on Ocean,Offshore and Arctic Engineering, San Francisco, California, 2014. June 8â€"13.
[9] A.J. Goupee, B.J. Koo, R.W. Kimball, K.F. Lambrakos, H.J. Dagher, Experimental comparison of three floating wind turbine concepts, J. Offshore Mech. Arctic Eng. 136 (2) (2014), 020906.
[10] H.R. Martin, R.W. Kimball, A.M. Viselli, A.J. Goupee, Methodology for wind/wave basin testing of floating offshore wind turbines, J. Offshore Mech. Arctic Eng. 136 (2) (2014), 020905.
[11] K. Karikomi, M. Ohta, A. Nakamura, S. Iwasaki, Y. Hayashi, A. Honda, Wind tunnel testing on negative-damped responses of a 7MW floating offshore wind turbine, in: Poster Presented at EWEA Offshore 2015, Copenhagen, 2015.
[12] A. Hansen, R. Laugesen, H. Bredmose, R. Mikkelsen, N. Psichogios, Small scale experimental study of the dynamic response of a tension leg platform wind turbine, J. Renew. Sustain. Energy 6 (5) (2014), 053108.
[13] H. Bredmose, R. Mikkelsen, A. Hansen, R. Laugesen, N. Heilskov, B. Jensen, J. Kirkegaard, Experimental study of the DTU 10MW wind turbine on a TLP floater in waves and wind, in: Presented at the EWEA Offshore 2015 Conference, 2015.
[14] H. Bredmose, F. Lemmer, M.B. Borg, A.M. Pegalajar-Jurado, R.F. Mikkelsen, T.S. Larsen, T. Fjelstrup, W. Yu, A.K. Lomholt, L. Boehm, J.A. Armendariz, The Triple Spar campaign: model tests of a 10MW floating wind turbine with waves, wind and pitch control, Energy Procedia 137 (2017) 58—76.
[15] W. Yu, F. Lemmer, H. Bredmose, M. Borg, A. Pegalajar-Jurado, R.F. Mikkelsen, T.S. Larsen, T. Fjelstrup, A.K. Lomholt, L. Boehm, D. Schlipf, J.A. Armendariz, The Triple Spar Campaign: Implementation and Test of a Blade Pitch Controller on a Scaled Floating Wind Turbine Model, ELSEVIER SCIENCE BV, 2017.
[16] R. Laugesen, A.M. Hansen, Experimental Study of the Dynamic Response of the DTU 10 MW Wind Turbine on a Tension Leg Platform, Master's thesis, Department of Wind Energy, Technical University of Denmark, DK2800 Lyngby, 2015. Denmark DTU Wind Energy M-0065, Master Thesis Report.
[17] R.F. Mikkelsen, The DTU 10MW 1:60 Model Scale Wind Turbine Blade, Tech. Rep., DTU Wind Energy, 2015.
[18] M.H. Hansen, L.C. Henriksen, Basic DTU Wind Energy Controller, Tech. Rep., DTU Wind Energy, 2013.
[19] C. Bak, F. Zahle, R. Bitsche, T. Kim, A. Yde, L.C. Henriksen, P.B. Andersen, A. Natarajan, M.H. Hansen, Description of the DTU 10 MW Reference Wind Turbine, Tech. Rep.,, DTU Wind Energy, 2013. Report-I-0092.
[20] F.J. Madsen, T.R.L. Nielsen, Experimental and Numerical Study of the Scaled DTU 10MW Floating Wind Turbine on a TLP Platform, Master's thesis, Department of Wind Energy, Technical University of Denmark, DK2800 Lyngby, Denmark, 2017.
[21] A. Pegalajar-Jurado, A.M. Hansen, R. Laugesen, R.F. Mikkelsen, M. Borg, T. Kim, N.F. Heilskov, H. Bredmose, Experimental and numerical study of a 10MW TLP wind turbine in waves and wind, J. Phys. Conf. 753 (2016), 092007.

[22] H. Bredmose, S. Larsen, D. Matha, A. Rettenmeier, E. Marino, L. Sættran, Collation of Offshore Windwave Dynamics: marine Renewables Infrastructure Network for Emerging Energy Technologies d2.4, Tech. Rep., DTU Wind Energy, 2012. deliverable of the Marinet project)

[23] T.J. Larsen, T.D. Hanson, A method to avoid negative damped low frequency tower vibrations for a floating pitch regulated wind turbine, J. Phys. Conf. 75 (2007), 012073). The Science of Making Torque from Wind.

[24] S. Schløer, H. Bredmose, A. Ghadirian, Analysis of experimental data: the average shape of extreme wave forces on monopile foundations and the NewForce model, Energy Procedia 137 (2017) 223–237.

[25] P.S. Tromans, A. Anaturk, P. Hagemeijer, A new model for the kinematics of large ocean waves - application as a design wave, in: Proc. 1st Int. Conf. 708 Offsh. Mech. And Polar Engng. (ISOPE), vol. 3, 1991, pp. 64–71, 1991.